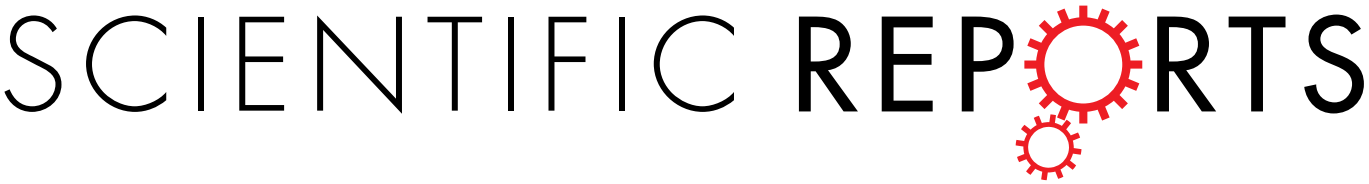

OPEN

Disordered RuO_2 exhibits two dimensional, low-mobility transport and a metal–insulator transition

Received: 12 June 2015
Accepted: 18 September 2015
Published: 26 February 2016

M. S. Osofsky[1], C. M. Krowne[2], K. M. Charipar[1], K. Bussmann[1], C. N. Chervin[3], I. R. Pala[3] & D. R. Rolison[3]

The discovery of low-dimensional metallic systems such as high-mobility metal oxide field-effect transistors, the cuprate superconductors, and conducting oxide interfaces (*e.g.*, $LaAlO_3/SrTiO_3$) has stimulated research into the nature of electronic transport in two-dimensional systems given that the seminal theory for transport in disordered metals predicts that the metallic state cannot exist in two dimensions (2D). In this report, we demonstrate the existence of a metal–insulator transition (MIT) in highly disordered RuO_2 nanoskins with carrier concentrations that are one-to-six orders of magnitude higher and with mobilities that are one-to-six orders of magnitude lower than those reported previously for 2D oxides. The presence of an MIT and the accompanying atypical electronic characteristics place this form of the oxide in a highly diffusive, strong disorder regime and establishes the existence of a metallic state in 2D that is analogous to the three-dimensional case.

The existence of metallic behavior reported for several 2D materials violates the famous prediction of Abrahams, Anderson, Licciardello, and Ramakrishnan[1] that all 2D systems must be localized regardless of the degree of disorder. The discovery of a metallic state in high-mobility metal oxide field-effect transistors (HMFET)[2–7] motivated several theoretical approaches that included electron–electron interactions to screen disorder. These models adequately described the results for low carrier concentration, high-mobility systems[8,9], but are not applicable to the case of highly disordered 2D metals. The HMFET results also motivated the development of a general scaling model for the 2D MIT that may also be applicable to highly disordered systems[10]. The presence of a metallic state in highly disordered 2D systems with very low mobility, the situation addressed by Abrahams *et al.*[1] indicates that either a modification of the existing theory[10] or a new theoretical approach for the 2D MIT is needed.

In conventional metals with low disorder, the metallic state is characterized by decreasing resistivity with decreasing temperature as described by the well-known Boltzmann or Bloch–Gruneisen transport theories. These theories are predicated on the existence of plane wave electrons with long mean free paths. Because disorder severely reduces the mean free path and the character of metallic transport changes, those models must be replaced with a quantum diffusion description. For highly disordered conductors in which resistivity does not decrease with decreasing temperature, a more fundamental definition of metallic transport is needed in which diffusive electrons extend throughout the material at $T = 0$. The disorder-driven MIT is then described as a quantum phase transition characterized by extended states for the metallic phase and by localized states for the insulating phase[11,12]. In three dimensions, the phase diagram has four regions[13]: insulating, critical, amorphous metal, and conventional metal (Fig. 1) with the observed properties determined by the position of the Fermi energy. It should be noted that this model is not rigorously correct due to the use of the density of states in the conductance in scaling relations for the renormalization group. However, it has proven to be a useful model for analyzing experimental data (see references 11, 14, and 15). In the conventional metal region, transport is controlled by electron–phonon scattering as described in the usual manner by Boltzmann transport with

[1]Materials and Sensors Branch (Code 6360), U.S. Naval Research Laboratory, Washington, DC 20375, USA. [2]Electromagnetics Technology Branch (Code 6850), U.S. Naval Research Laboratory, Washington, DC 20375, USA. [3]Surface Chemistry Branch (Code 6170), U.S. Naval Research Laboratory, Washington, DC 20375, USA. Requests for materials should be addressed to D.R.R. (email: rolison@nrl.navy.mil). Correspondence should be addressed to M.S.O. (email: michael.osofsky@nrl.navy.mil)

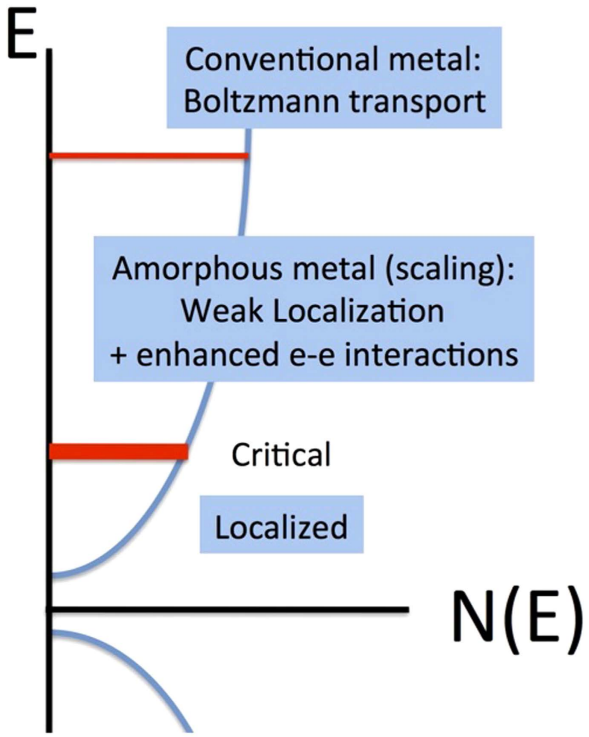

Figure 1. Schematic of the generic phase diagram for the metal–insulator transition. The continuous transition from amorphous to conventional metal phases is represented by a line in this rendering.

conductivity increasing with decreasing temperature. In the amorphous metal region, transport is controlled by weak localization with enhanced electron–electron interactions where conductivity follows the square root of temperature ($\sigma = \sigma_0 + \sigma_1 T^{½}$)[11,13–16]. Here, the electronic conductivity drops with decreasing temperature, but extrapolates to a finite value at $T = 0$.

The 2D case is quite different. The original theoretical work that described the 3D MIT[1] also predicted that all 2D systems will be insulators with $\sigma \sim \log(T)$. Later work indicated that this log(T) behavior would also be a consequence of enhanced electron–electron interactions in a diffusive 2D system[17]. Indeed, conductivity that followed log(T) behavior was observed for Si MOSFETs[18,19] and ultrathin films[20–24] (~10-nm thick). A drawback arises when using either the thin film or transistor-based systems to explore the match of experimental results to log(T) behavior because the effective thickness of the conducting layer varies either due to changing film thickness or the spatial extent of the gated charge layer in the FET. Later work on Si HMFETs and other systems[2–7] indicated that an MIT was actually possible in 2D systems. Some of these results were modeled using a renormalization group theory of electron–electron interactions where high-mobility carriers present at low carrier concentration screen the lattice disorder[8]. A reexamination of the original scaling arguments of reference 1 concluded that a 2D MIT was indeed possible for any level of disorder[10].

Preparing disordered RuO_2 and tuning the transport properties

To study the highly disordered case, we prepared disordered 10-, 20-, and 30-nm thick films of ruthenium dioxide, RuO_2, which in its anhydrous rutile crystalline form is a high carrier concentration metallic oxide ($n \sim 10^{23}\,cm^{-3}$). These film-thickness values (verified by atomic force microscopy) are consistent with systems that exhibited 2D behavior such as the 40-nm–thick disordered $Si_{1-x}Au_x$ films[16] and interfacial oxides[25]. The high cost of ruthenium has motivated our development of a liquid-phase, subambient temperature technique to synthesize ultrathin films of ruthenium dioxide[26,27] for applications in which the properties are surface-dominated such as charge storage for pulse power[28] and electrocatalysis[26,29,30]. On planar substrates, ~10 nm of oxide is deposited (designated RuO_2 nanoskin); repeating the solution-phase deposition adds an additional 10-nm of oxide per cycle. Previous work demonstrated that the close-packed nanoparticulate morphology of the RuO_2 nanoskin is unchanged with calcination up to at least 200 °C in air or argon. The X-ray photoelectron (XPS) and diffraction (XRD) results from the same study show that the chemical state and atomic structure of the RuO_2 remains invariant up to 200 °C[27]. After deposition, the films were patterned using a 266-nm diode-pumped solid-state laser into a configuration that enabled standard four-probe resistivity and Hall measurements (Fig. 2(a) inset). Hall measurements were made in a Quantum Design Physical Property Measurement System (PPMS) between 1.75 K and 305 K for $-8T \leq B \leq 8T$.

To access higher conductivity regions of the metallic rutile phase and serve as a crystalline control for the solution-deposited ruthenia, 10- 20- and 30-nm–thick RuO_2 films were deposited onto SiN/Si substrates held at 600 °C by reactive sputtering from a Ru metal target in a 2:1 ratio of $Ar:O_2$ at a pressure of 3 mTorr. The XRD analysis of the physically sputtered films showed crystalline rutile RuO_2 and no other competing phases. These

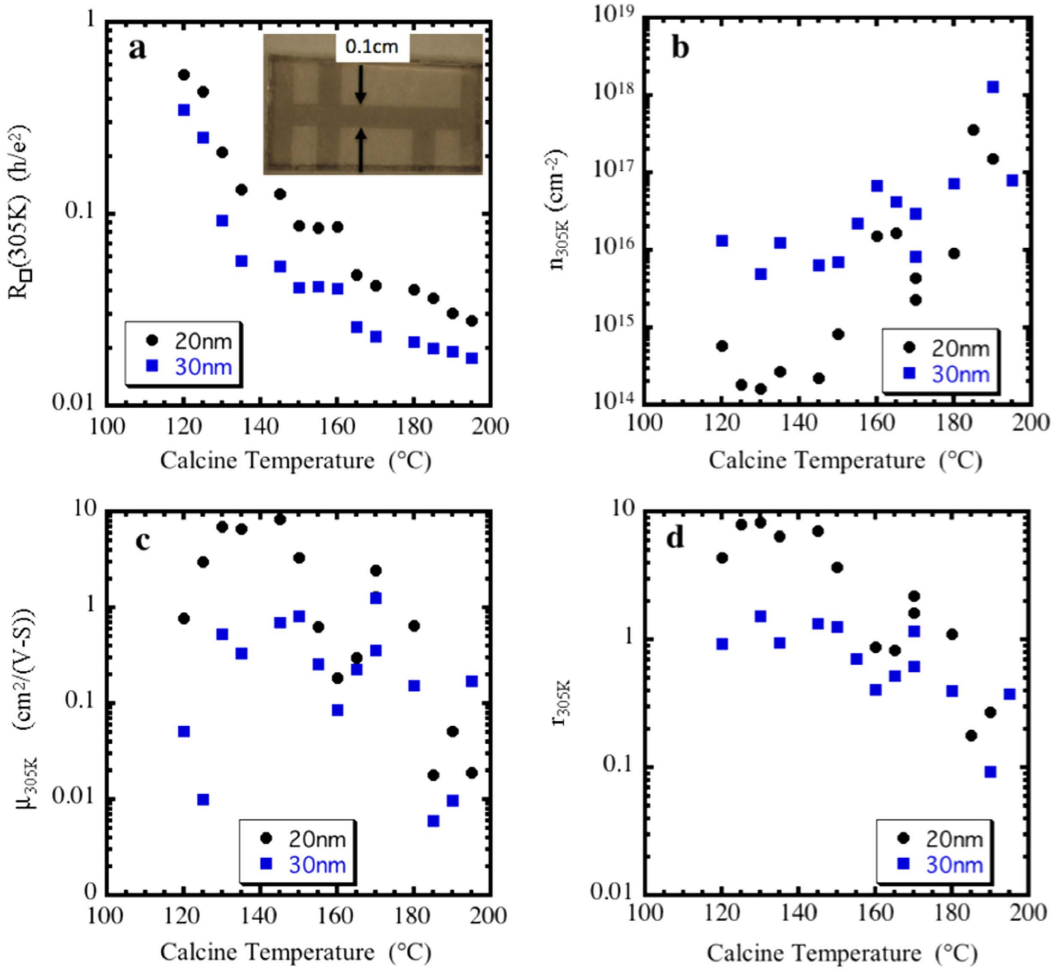

Figure 2. Room-temperature transport properties of RuO_2 nanosheets. (**a**) R/□ (plotted in units of quantum resistance, h/e^2); (**b**) carrier concentration; (**c**) mobility; and (**d**) the "r_s" parameter (labeled r_{305K}) as a function of calcination temperature for the 20-nm (on SiO_2 substrate) and 30-nm (on Al_2O_3 substrate) thick RuO_2 nanosheets. Inset (**a**) geometry of the laser-patterned films.

films, denoted as "sputter 1" and "sputter 2", exhibit conventional metallic behavior with resistance decreasing with decreasing temperature (inset, Fig. 3).

As grown on 3D-structured substrates and on planar, smooth substrates the solution-deposited films consist of uniform, high-impedance, X-ray amorphous 2–3-nm grains[26,27]. By calcining at moderate temperatures (~100–200 °C), the RuO_2 nanoskins retain their X-ray amorphous structure (see supplemental information), yet exhibit a decrease in resistivity to that characteristic of a disordered metal, less than 1 mΩ−cm. The equivalent 2D resistance is almost two orders of magnitude lower than the quantum resistance per square, h/2e^2, at room temperature (Fig. 2a). The RuO_2 nanoskins can thus be driven through the MIT by systematically calcining at increasing temperatures *without changing the thickness* (Fig. 3). This shape invariance makes this system ideal for studies of the two-dimensional MIT.

2D vs. 3D transport

The temperature-dependent electronic transport data were plotted as conductivity *vs.* $T^{1/2}$, the expected relationship for 3D behavior, because conductivity is the relevant quantity for determining whether a material is a metal or an insulator. The 3D behavior was considered first because a 2D MIT was not anticipated for these ultrathin films. While there is a clear increase in the overall values of the conductivity with calcination temperature and a clear transition from insulating to metallic states similar to that seen in disordered FETs[31], the curves clearly do not fit the 3D temperature dependence of $T^{½}$ (Fig. 4).

When plotting the conductance data as a function of log(T), the behavior expected for homogeneously disordered 2D systems[11] and granular systems[32], yields a better fit to the data (Fig. 5). Because the RuO_2 nanoskins consist of amorphous grains as determined by electron diffraction[27] and grazing-incidence XRD (supplemental information) rather than metallic particles embedded in an insulating matrix, it is apparent that they must be treated as a uniform disordered system rather than as a granular metal. This structural assignment is confirmed by the continuous increase in carrier concentration with calcination (Fig. 2b). The presence of granular behavior

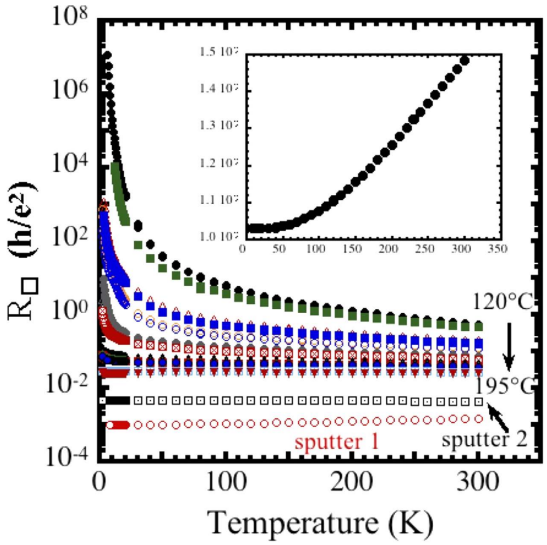

Figure 3. Sheet resistance as a function of temperature of thin-film disordered and crystalline RuO_2. R/□ (plotted in units of quantum resistance, h/e^2) obtained from 1.75 to305 K for 20-nm solution-deposited RuO_2 nanosheet as a function of calcination temperature. Inset: blow-up of the data for a 20-nm sputtered RuO_2 film on a SiN/Si substrate grown at 600 °C (sputter 1) that exhibits conventional metallic behavior with resistance decreasing with decreasing temperature.

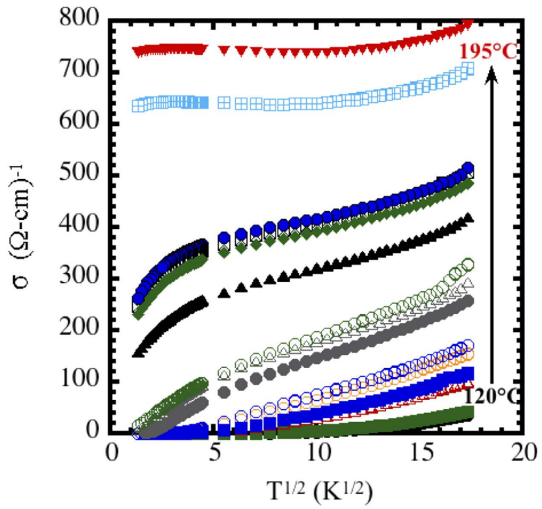

Figure 4. Plotting the conductivity data to the $T^{½}$ behavior expected for three-dimensional systems near the MIT.

can also be ruled out because granular systems exhibit $\sigma \sim \log(T)$ at high temperatures and transport properties characteristic of disordered metals, *i.e.*, weak-localization and enhanced electron-electron interactions, at low temperatures[32]. It is clear from Fig. 5 that the log(T) behavior only manifests at low temperatures.

Several features are evident from these plots. For RuO_2 nanoskins that were calcined at the highest temperatures, the conductance is metallic with flat temperature dependences at low temperatures. For lower-temperature calcinations (between 180 °C and 190 °C for the 20-nm–thick nanoskins and between 160 °C and 165 °C for the 30-nm–thick nanoskins; supplemental material) there is a transition from the metallic to a weakly localized insulator phase with $\sigma \sim \log(T)$. This type of "transition," where the slope of the temperature dependence changes, is often identified as the MIT and was predicted to occur for $\rho \sim 200\,\mu\Omega$-cm in 3D[13]. Finally, the temperature dependence changes to a more severe localized behavior for the lowest calcination temperatures (between 160 °C and 165 °C for the 20-nm–thick nanoskins and between 140 °C and 145 °C for the 30-nm–thick nanoskins). This change in transport behavior signifies the transition in these ultrathin films from weakly localized carriers to strongly localized insulators[19].

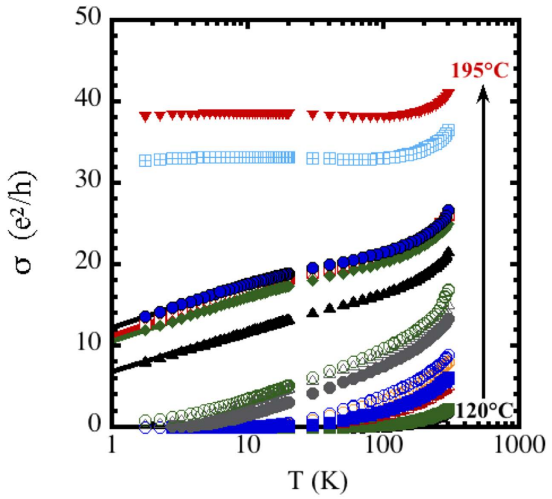

Figure 5. Plotting the conductivity data to the log(T) behavior expected for two-dimensional systems near the MIT. Conductivity per □ for the 20-nm thick RuO_2 nanosheets plotted *vs*. log(T) as a function of calcination temperature. The samples were calcined from 120 °C to 195 °C in 5° steps (185 °C data are not included). The symbols are the same as in Fig. 4. The solid lines are extrapolated fits to $\sigma = \sigma_0 + \sigma_1 \log(T)$ for $T < 10$ K.

These curves clearly show that the RuO_2 nanoskins exhibit 2D transport characteristics at low temperatures. The relevant low-temperature data were fitted to

$$\sigma = \sigma_0 + \sigma_1 \log(T) \quad (1)$$

a generic function that describes 2D conductivity in disordered metals[11]. The fits are shown as solid lines in Fig. 5. Estimates of the phase coherence length for the metallic samples indicate that films can be treated as 2D systems (supplemental Information).

One of the key issues in understanding the MIT is the slope of the so-called "mobility edge," the critical phase line that describes the scaling of the MIT. Early work by Mott[33] on 3D systems suggested that this line is discontinuous and that an abrupt transition occurs from the metal to insulating phases (hence the term "edge"). Later work showed that this transition is continuous. In three dimensions, this line is usually defined as the relationship between a driving parameter, generically labeled as p, and σ_0^{3D}, the value of conductivity extrapolated to $T = 0$[11–16]. The usual formulation is $\sigma_0^{3D} \sim (p - p_c)^{\nu}$ where p_c is the critical value of p (*i.e.*, where $\sigma_0^{3D} = 0$) and where ν is a critical exponent[1,11–16,34]. Experimentally, p is often the carrier concentration. Another choice for p is the bare conductivity that can be approximated by the room-temperature conductivity[14]. It has been shown that in three dimensions, $\nu = ½$ in Si:P[35], while $\nu = 1$ in disordered metals[11,13–16].

In two dimensions, the analogue to the "amorphous metal" phase shown in Fig. 1 is an atypical insulator phase and this analysis is complicated by the fact that the data cannot be extrapolated to $T = 0$. In this case, one can replace σ_0 from equation (1) with σ_{1K} so that $\sigma_{1K}^{2D} \sim (\sigma_{300K} - \sigma_c)^{\nu}$ where σ_c is the value of σ_{300K} for which $\sigma_{1K} = 0$. The mobility edges for the three thicknesses of solution-deposited RuO_2 are plotted in Fig. 6. These plots clearly show that the transition is continuous with $\nu = 1$, similar to many disordered 3D systems.

High carrier concentration and low mobility

The sheet carrier concentration at 305 K, as determined from Hall measurements, increased from $n \sim 10^{14}$–10^{16} cm^{-2} for the insulating samples to 10^{17}–10^{18} cm^{-2} for the most conductive ones (Fig. 2b). Most of the calcinations produced films with hole carriers but several resulted in electron carriers. This variability in the dominant charge carrier is consistent with earlier work on thin-film RuO_2 and is attributed to oxygen defects[36,37]. These values of carrier concentration are orders of magnitude larger than those reported for HMFETs (~10^{10}–10^{12} cm^{-2})[2–7,31] with the metallic samples having bulk values comparable to conventional metals ($n_{3D} \sim 10^{23}$ cm^{-3}). In the HMFET systems, the critical carrier densities were reported to be ~10^{10}–10^{12} cm^{-2} while we find n~10^{16} cm^{-2} for the transitions from strongly localized to weakly localized, log(T), behavior.

The calculated room-temperature mobility of the carriers in RuO_2 nanoskins as a function of calcination temperature shows significant scatter between ~0.01–10 $cm^2/(V\text{-}s)$ with the most metallic samples (those calcined at the highest temperature) exhibiting mobility between ~0.1 and 0.01 $cm^2/(V\text{-}s)$ (Fig. 2c). While these values are comparable to some reported for interfacial oxides[38–41], they are many orders of magnitude smaller than those reported for HMFET devices, ~10^4 $cm^2/(V\text{-}s)$[2–4,6,7,31]. The values are also orders of magnitude smaller than those recently reported in gated structures for single- and double-layer MoS_2, which exhibits an MIT with carrier concentrations on the order of 10^{13} cm^{-2} and mobilities that are in the range of 1–1000 $cm^2/(V\text{-}s)$[42–45]. Although the carriers in the RuO_2 nanoskins are present at high concentrations, approaching those of metals, their low mobility does not track that expected of metals, again highlighting the high disorder in the nanoscale oxide derived from the low-temperature solution-deposition protocol.

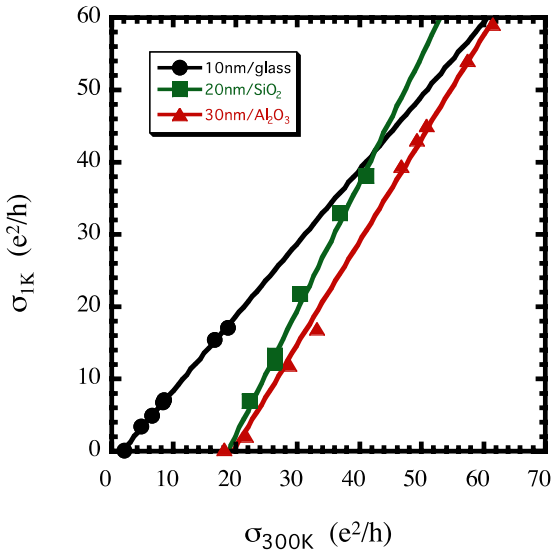

Figure 6. Continuity of the conductivity as disordered RuO_2 nanosheets approach the MIT. Conductivity at 1 K vs. conductivity at 300 K exhibits the linear "mobility edge" observed in many three-dimensional systems. Note that the single-layer data are from several samples prepared together in the same deposition batch.

The quantity $r_s = E_{e-e}/E_F$, where E_{e-e} is the characteristic electron–electron interaction energy and E_F is the Fermi energy, has been used to characterize transport in 2D systems[2–7,46–48]. While this quantity does not take into account disorder, the bare (high temperature), unrenormalized, value is useful for comparison with the other systems that have been studied. The parameter can be expressed as:

$$r_s = \frac{1}{\sqrt{\pi n_0^{2D}[a_B^*]^2}} \quad (2)$$

where a_B^* is the Bohr radius, $\frac{\hbar^2}{m_{electron}e^2}$, and n_0^{2D} is the sheet carrier concentration[48]. We find $r_{305K} \sim 1$–10 for the insulating samples and 0.1–0.3 for the most conductive ones (Fig. 2d). The transition from strongly localized to weakly localized, log(T), behavior occurs for $r_{305K} \sim 1$ for both the 20- and 30-nm–thick RuO_2 nanoskins. The transition from weakly localized to metallic behavior occurs for $r_{305K} \sim 0.2$ for the 20-nm–thick film and 0.5 for the 30-nm–thick film; in contrast the interfacial oxides have values of ~5–35 at the MIT[2,4]. It is not surprising that the critical values of r_s for the two situations are so different in that the levels of disorder are so different.

The strong deviation of the values of the bare carrier concentration, mobility, and r_s of these RuO_2 films from those of the previously studied 2D systems leads us to conclude that disordered RuO_2 exhibits a 2D MIT that falls in an as yet, unexplored region of transport phase space. The nature of the 2D MIT in the ballistic case has still not been definitely determined (*i.e.*, whether it is a "true" quantum phase transition or due to "conventional disorder")[49,50]. Regardless of the microscopic details of the MIT, combining the HMFET results with those for the highly diffusive case presented here, it becomes clear that the 2D MIT is ubiquitous in the entire range of disorder.

2D phase diagram analogous to 3D

Several scaling approaches have been developed to describe transport in disordered 2D conductors[11,12,51–54]. The two phenomena modeled in these theories, weak localization and enhanced electron–electron interactions, are predicated on the presence of strong disorder, *i.e.*, highly diffusive transport, and are thus distinct from those developed for the HMFET results, which are in the ballistic limit. They all predict insulating behavior in two dimensions and are therefore, inadequate to describe the results reported here. Our results clearly show that the phase diagram of the 2D MIT for highly disordered, high carrier concentration materials is analogous to that for the 3D case shown in Fig. 1 with the amorphous metal phase replaced with an amorphous insulator phase that is characterized by the conductivity having a log(T) dependence. These results are consistent with more recent theory showing that a 2D MIT is possible, although it would need to be modified to apply to the highly disordered case[10].

In summary, we have provided conclusive evidence for a continuous 2D metal–insulator transition in a low mobility, high carrier concentration material, highly disordered RuO_2 nanoskins, findings that contradict the seminal work by Abrahams *et al.*[1] The 2D metallic behavior occurs in a regime where mobility is orders of magnitude lower and carrier concentration is orders of magnitude larger than those observed in the previous systems that expressed 2D MITs, thus expanding the range of observed 2D metallic behavior. Our findings support more recent scaling arguments that predict a metallic state in 2D systems, and are key to understanding the transport properties of low-dimensional systems such as interfacial oxides.

References

1. Abrahams, E., Anderson, P. W., Licciardello, D. C. & Ramakrishnan, T. V. Scaling theory of localization: Absence of quantum diffusion in two dimensions. *Phys. Rev. Lett.* **42,** 673–676 (1979).
2. Kravchenko, S. V., Kravchenko, G. V., Furneaux, J. E., Pudalov, V. M. & D'Iorio, M. Possible metal–insulator transition at B = 0 in 2 dimensions. *Phys. Rev. B* **50,** 8039–8042 (1994).
3. Hanein, Y. *et al.* The metallic like conductivity of a two-dimensional hole system. *Phys. Rev. Lett.* **80,** 1288–1291 (1998).
4. Yoon, Y., Li, C. C., Shahar, D., Tsui, D. C. & Shayegan, M. Wigner crystallization and metal–insulator transition of two-dimensional holes in GaAs at B=0. *Phys. Rev. Lett.* **82,** 1744–1747 (1999).
5. Simmons, M. Y. *et al.* Weak localization, hole–hole interactions, and the "metal"–insulator transition in two dimensions. *Phys. Rev. Lett.* **84,** 2489–2492 (2001).
6. Hamilton, A. R. *et al.* Reentrant insulator–metal-insulator transition at B=0 in a two-dimensional hole gas. *Phys. Rev. Lett.* **82,** 1542–1545 (1999).
7. Qiu, R. L. J., Gao, X. P. A., Pfeiffer, L. N. & West, K. W. Connecting the reentrant insulating phase and the zero-field metal–insulator transition in a 2D hole system. *Phys. Rev. Lett*. **108,** 106404 (2012).
8. Punnoose, A. & Finkel'stein, A. M. Metal–insulator transition in disordered two-dimensional electron systems. *Science* **310,** 289–291 (2005).
9. Anissimova, S. Kravchenko, S. V., Punnoose, A., Finkel'stein, A. M. & Klapwijk, T. M. Flow diagram of the metal–insulator transition in two dimensions. *Nature Phys*. **3,** 707–710 (2007).
10. Dobrosavljević, V., Abrahams, E., Miranda, E. & Chakravarty, S. Scaling theory of two-dimensional metal–insulator transitions. *Phys. Rev. Lett.* **79,** 455 (1997).
11. Lee, P. A. & Ramakrishnan, T. V. Disordered electronic systems. *Rev. Mod Phys.* **57,** 287–337 (1985).
12. Belitz, D. & Kirkpatrick, T. R. The Anderson–Mott transition. *Rev. Mod. Phys.* **66,** 261–380 (1994).
13. McMillan, W. L. Scaling theory of the metal–insulator transition in amorphous materials. *Phys. Rev. B* **24,** 2739–2743 (1981).
14. Osofsky, M., Tardy, H., LaMadrid, M. & Mochel, J. M. Strong and weak electron spin-orbit scattering near the metal–insulator transition. *Phys. Rev. B* **31,** 4715–4717 (1985).
15. Hertel, G., Bishop, D. J., Spencer, E. G., Rowell, J. M. & Dynes, R. C. Tunnelling and transport measurements at the metal–insulator transition of amorphous Nb:Si. *Phys. Rev. Lett*. **50,** 743–746 (1983).
16. Nishida, N. *et al.* Transport properties of amorphous $Si_{1-x}Au_x$: Metal–insulator transition and superconductivity. *J. Non-Cryst. Solids* **59&60,** 149–152 (1983).
17. Altshuler, B. L. & Aronov, A. G. in *Electron–Electron Interactions in Disordered Systems* (eds Efros, A. L. & Pollak, M.) 1–154 (North Holland, 1985).
18. Bishop, D. J., Tsui, D. C. & Dynes, R. C. Nonmetallic conduction in electron inversion layers at low temperatures. *Phys. Rev. Lett.* **44,** 1153–1156 (1980).
19. Minkov, G. M. *et al.* The conductivity of disordered 2D systems: from weak to strong localization. 10th International Symposium on Nanostructures: Physics and Technology, Zhores I. Alferov, L.E., Editors, *Proceedings of SPIE* **5023**, 482–485 (2003).
20. Dolan, G. J. & Osheroff, D. D. "Nonmetallic conduction in thin metal films at low temperatures. *Phys. Rev. Lett*. **43,** 721–724 (1979).
21. Abraham, D. & Rosenbaum, R. Localization in thin copper films. *Phys. Rev. B* **27,** 1409–1416 (1983).
22. Beutler, D. E. & Giordano, N. Localization and electron–electron interaction effects in thin Bi wires and films. *Phys. Rev. B* **38,** 8–19 (1988).
23. Van den dries, L., Van Haesendonck, C., Bruynseraede, Y. & Deutscher, G. Two-dimensional localization in thin copper films. *Phys. Rev. Lett.* **46,** 565–568 (1981).
24. Bergmann, G. Weak localization in thin films: a time-of-flight experiment with conduction electrons. *Phys. Rep*. **107,** 1–58 (1984).
25. Basletic, M. *et al.* Mapping the spatial distribution of charge carriers in $LaAlO_3/SrTiO_3$ heterostructures. *Nature Mater*. **7,** 621–625 (2008).
26. Ryan, J. V. *et al.* Electronic connection to the interior of a mesoporous insulator with nanowires of crystalline RuO_2. *Nature* **406,** 169–172 (2000).
27. Chervin, C. N. *et al.* Making the most of a scarce platinum-group metal: conductive ruthenia nanoskins on insulating silica filter paper. *Nano Lett.* **9,** 2316–2321 (2009).
28. Chervin, C. N., Lubers, A. M., Long, J. W. & Rolison, D. R. Effect of temperature and atmosphere on the conductivity and electrochemical capacitance of single-unit-thick ruthenium dioxide. *J. Electroanal. Chem*. **644,** 155–163 (2010).
29. Sassin, M. B., Chervin, C. N., Rolison, D. R. & Long, J. W. Redox deposition of nanoscale metal oxides on carbon for next-generation electrochemical capacitors. *Acc. Chem. Res.* **46,** 1062–1074 (2013).
30. Pietron, J. J., Pomfret, M. B., Chervin, C. N., Long J. W. & Rolison, D. R. Direct methanol oxidation at low overpotentials using Pt nanoparticles electrodeposited at ultrathin conductive RuO_2 nanoskins. *J. Mater. Chem.* **22,** 5197–5204 (2012).
31. Kravchenko, S. V. & Sarachik, M. P. Metal–insulator transition in two-dimensional electron systems. *Rep. Progr. Phys.* **67,** 1–44 (2004).
32. Beloborodov, I. S., Lopatin, A. V., Vinokur, V. M. & Efetov, K. B. Granular electronic systems. *Rev. Mod. Phys*. **79,** 469–518 (2007).
33. Mott, N. F. *Metal–Insulator Transitions* (Taylor and Francis, 1974).
34. Rosenbaum, T. F., Andres, K., Thomas, Q. A. & Lee, P. A. Conductivity cusp in a disordered metal. *Phys. Rev. Lett.* **46,** 568–571 (1981).
35. Paalanen, M. A., Rosenbaum, T. F., Thomas, G. A. & Bhatt, R. N. Stress tuning of the metal–insulator transition at millikelvin temperatures. *Phys. Rev. Lett*. **48,** 1284–1287 (1982); Thomas, G.A., Paalanen, M. & Rosenbaum, T.F. Measurements of conductivity near the metal–insulator critical point. *Phys. Rev. B* **27**, 3897–3900 (1983).
36. Tong, K. Y., Jelenkovic, V., Cheung, W. Y. & Wong, S. P. Temperature dependence of resistance in reactively sputtered RuO_2 thin films. *J. Mater. Sci. Lett.* **20,** 699–700 (2001).
37. Steeves, M. M. & Lad, R. J. Influence of nanostructure on charge transport in RuO_2 thin films. *J. Vac. Sci. Technol. A* **28,** 906–911 (2010).
38. Fix, T., Schoofs, F., MacManus-Driscoll, J. L. & Blamire, M. G. Charge confinement and doping at $LaAlO_3/SrTiO_3$ interfaces. *Phys. Rev. Lett.* **103,** 166802 (2009).
39. Hotta, Y., Susaki, T. & Hwang, H. Y. Polar discontinuity doping of the $LaVO_3/SrTiO_3$ interface. *Phys. Rev. Lett.* **99,** 236805 (2007).
40. Breckenfeld, E. *et al.* Effect of growth induced (non)stoichiometry on interfacial conductance in $LaAlO_3/SrTiO_3$. *Phys. Rev. Lett.* **110,** 196804 (2013).
41. Wong, F. J., Chopdekar, R. V. & Suzuki, Y. Disorder and localization at the $LaAlO_3/SrTiO_3$ heterointerface. *Phys. Rev. B* **82** 165413 (2010).
42. Baugher, B. W. H., Churchill, H. O. H., Yang, Y. & Jarillo-Herrero, P. Intrinsic Electronic Transport Properties of High-Quality Monolayer and Bilayer MoS_2. *Nano Lett.* **13,** 4212–4216 (2013).
43. Radisavljevic, B. & Kis, A. Mobility engineering and a metal–insulator transition in monolayer MoS_2. *Nat. Mat*. **12,** 815–820 (2013).
44. Schmidt, H. *et al.* Transport Properties of Monolayer MoS_2 Grown by Chemical Vapor Deposition. *Nano Lett.* **14,** 1909–1913 (2014).
45. Chen, X. *et al.* Probing the electron states and metal-insulator transition mechanisms in molybdenum disulphide vertical heterostructures, *Nat. Commun.* **6:6088** doi: 10.1038/ncomms7088.
46. Tanatar, B. & Ceperley, D. M. Ground state of the two-dimensional electron gas. *Phys. Rev. B* **39,** 5005–5016 (1989).

47. Wilamowski, Z., Sandersfeld, N., Jantsch, W., Többen, D. & Schäffler, F. Screening breakdown on the route toward the metal–insulator transition in modulation doped Si/SiGe quantum wells. *Phys. Rev. Lett.* **87,** 026401 (2001).
48. Spivak, B., Kravchenko, S. V., Kivelson, S. A. & Gao, X. P. A. *Colloquium*: Transport in strongly correlated two dimensional electron fluids. *Rev. Mod. Phys.* **82,** 1743–1766 (2010).
49. Altshuler, B. L., Maslov, D. L. & Pudalov, V. M. Metal–insulator transition in 2D: resistance in the critical region. *Physica E* **9,** 209–225 (2001).
50. Sondhi, S. L., Girvin S. M., Carini, J. P. & Shadar, D. Continuous quantum phase transitions. *Rev. Mod. Phys.* **69,** 315–333 (1997).
51. Altshuler, B. L. & Aronov, A. G. Fermi-liquid theory of the electron–electron interaction effects in disordered metals. *Solid State Commun.* **46,** 429–435 (1983).
52. Castellani, C., Di Castro, C., Lee, P. A. & Ma, M. Interaction-driven metal-insulator transitions in disordered fermion systems. *Phys. Rev. B* **30,** 527–543 (1984).
53. Finkelshtein, A. M. Spin fluctuations in disordered systems near the metal–insulator transition. *Zh. Eksp. Teor. Fiz. Pis'ma Red.* **40,** 63 (1984) [*Sov. Phys. JETP Lett.* **40**, 796 (1984)].
54. Kirkpatrick, T. R. & Belitz, D. Existence of a phase transition in Finkelshtein's model for a disordered Fermi liquid. *Phys. Rev. B* **40,** 5227–5230 (1989).

Acknowledgements

This work was supported by the Office of Naval Research. The authors wish to acknowledge Steve Hair for providing data processing software. I.R.P. acknowledges the U.S. National Research Council for a Postdoctoral Fellowship (2012–2015).

Author Contributions

D.R.R. initiated the project and oversaw experimental design. M.S.O. designed and performed the transport measurements. M.S.O. and C.M.K. analyzed the data using formalisms for transport in 2D and 3D. C.N.C. and I.R.P. prepared the solution-deposited disordered RuO_2 nanoskins and obtained structural and thickness measurements. K.M.B. prepared the reactive sputtered polycrystalline thin RuO_2 films and obtained structural and thickness measurements. K.M.C. patterned both types of films for four-point terminal transport measurements.

Additional Information

Supplementary information accompanies this paper at http://www.nature.com/srep

Competing financial interests: The authors declare no competing financial interests.

How to cite this article: Osofsky, M. S. *et al.* Disordered RuO_2 exhibits two dimensional, low-mobility transport and a metal-insulator transition. *Sci. Rep.* **6**, 21836; doi: 10.1038/srep21836 (2016).